High-temperature superconductivity in atomic metallic hydrogen

Jeffrey M. McMahon and David M. Ceperley

High-Temperature Superconductivity in Atomic Metallic Hydrogen

Jeffrey M. McMahon[1, *] and David M. Ceperley[1, 2, †]

[1]*Department of Physics, University of Illinois at Urbana-Champaign, Illinois 61801, USA*
[2]*NCSA, University of Illinois at Urbana-Champaign, Illinois 61801, USA*
(Dated: September 12, 2011)

Superconductivity in the recently proposed ground-state structures of atomic metallic hydrogen is investigated over the pressure range 500 GPa to 3.5 TPa. Near molecular dissociation, the electron–phonon coupling λ and renormalized Coulomb repulsion are similar to the molecular phase. A nearly continuous increase in the critical temperature T_c with pressure is thus found in this range, to $\sim$356K near 500 GPa. As the atomic phase stabilizes with increasing pressure, λ increases, causing T_c to approach 481K near 700 GPa. At the first atomic–atomic structural phase transformation near $1 - 1.5$ TPa, a discontinuous jump in λ occurs, causing a significant increase in T_c of up to 764K.

I. INTRODUCTION

At relatively low pressures, hydrogen exists in an insulating molecular phase. In 1935, Wigner and Huntington predicted that sufficient pressure would cause both a molecular-to-atomic transition and metallization[1]. Recent *ab initio* calculations support these predictions, and have revealed the precise details associated with both effects. Calculations based on *ab initio* random structure searching by Pickard and Needs[2] as well as McMahon and Ceperley[3] suggest that the molecular-to-atomic transition occurs near 500 GPa, the latter study also revealing a profusion of structures that atomic hydrogen adopts; and exact-exchange calculations based on density-functional theory (DFT) by Städele and Martin[4] suggest a metallization pressure of at least 400 GPa. In 1968, Ashcroft predicted an even further transition in high-pressure hydrogen, a metallic-to-superconducting one[5]. Within the framework of Bardeen–Cooper–Schrieffer (BCS) theory[6], three key arguments support this prediction: (i) the ions in the system are single protons, and their small masses cause the vibrational energy scale of the phonons to be remarkably high (e.g., $k_B \langle \omega \rangle \approx 2300$K near 500 GPa, where k_B is Boltzmann's constant and $\langle \omega \rangle$ is the average phonon frequency – see below), as is thus the prefactor in the expression for the critical temperature T_c; (ii) since the electron–ion interaction is due to the bare Coulomb attraction, the electron–phonon coupling should be strong; and (iii) at the high pressures at and above metallization, the electronic density of states $N(0)$ at the Fermi surface should be large and the Coulomb repulsion between electrons should be relatively low, typical features of a high-density system. These arguments will be revisited, and demonstrated to indeed be the case, below.

Ever since the prediction of high-T_c superconductivity in hydrogen[5], a large number of efforts have focused on determining the precise value(s) of T_c[7–22]. In the molecular phase, the high-pressure metallic *Cmca* structure (which transitions to the atomic phase[2,3]) has recently been studied in-depth[20–22], and shown to have a T_c that increases up to 242K near 450 GPa. In the atomic phase, estimations of T_c have varied widely, but in general suggest a large increase with pressure[7–19]. Early calculations suggested that $T_c \approx 135 - 170$K near 400 GPa (although, it is now believed that this is within the molecular phase[2,3], as discussed above)[14]; near $480 - 802$ GPa, more recent calculations suggest that $T_c \approx 282 - 291$K[18]; and near 2 TPa, calculations suggest that T_c can reach $600 - 631$K in the face-centered cubic (fcc) lattice[16,17]. The latter two studies will be discussed further below.

However, previous studies of superconductivity in atomic metallic hydrogen have simply assumed candidate ground-state structures, in a number of cases the fcc lattice[8–10,12,16,17]. Recently, McMahon and Ceperley demonstrated that such structures are incorrect, and provided a comprehensive picture of the (presumably correct) ground-state structures from 500 GPa to 5 TPa[3]. Molecular hydrogen was shown to dissociate near 500 GPa, consistent with the predictions of Pickard and Needs[2]. With increasing pressure, atomic hydrogen passes through two ground-state structural phases before transforming to a close-packed lattice, such as fcc or possibly the hexagonal close-packed (hcp) lattice. The first is a body-centered tetragonal structure with space-group $I4_1/amd$ (Hermann–Mauguin space-group symbol, international notation) with a c/a ratio greater than unity, as shown in Fig. 1. Including estimates of proton zero-point energies (ZPEs), $I4_1/amd$ was demonstrated to transform into a layered structure with space-group $R\text{-}3m$ near 1 TPa, also shown in Fig. 1, which is similar to a possible high-pressure phase of lithium[23]. $R\text{-}3m$ remains stable to $\sim$3.5 TPa, eventually compressing to a close-packed lattice. Given such novel crystal phases and that T_c can be very sensitive to structural details[11], as well as the fact that modern methods of calculating values of T_c should be more accurate than those used in earlier studies, it is of great interest to re-investigate the long-outstanding predictions of superconductivity in atomic metallic hydrogen.

This Article is outlined as follows: in Section II, the theoretical background used for estimating T_c in this work is
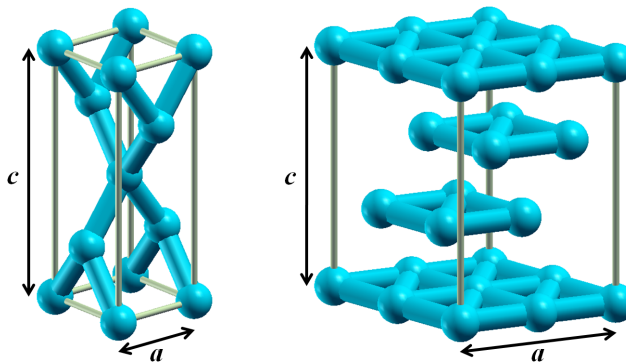
FIG. 1: (color online). Ground-state structures of atomic metallic hydrogen. (left) Conventional unit-cell of $I4_1/amd$ at 700 GPa. (right) $2 \times 2 \times 1$ supercell of R-$3m$ at 2 TPa. a and c parameters are shown in the figure, as discussed in the text. Fictitious bonds have been drawn for clarity.

presented; computational details are given in Section III; in Section IV, properties of the ground-state structures of atomic metallic hydrogen as a function of pressure, such as lattice parameters and vibrational properties influencing the $I4_1/amd \rightarrow R$-$3m$ transition, are presented and discussed; superconductivity is investigated in Section V; Section VI concludes.

II.   THEORETICAL BACKGROUND

According to the BCS theory of superconductivity[6], there is a simple relationship between T_c, $\langle\omega\rangle$, $N(0)$, and the pairing potential V arising from the electron–phonon interaction,

$$k_{\mathrm{B}}T_c = 1.14\langle\omega\rangle \exp\left[-\frac{1}{N(0)V}\right] \quad . \tag{1}$$

This relation is valid as long as $k_{\mathrm{B}}T_c \ll \langle\omega\rangle$, corresponding to weak coupling – see below.

McMillan later solved the finite-temperature Eliashberg equations for T_c[24], which including a correction by Dynes[25] can be written as

$$k_{\mathrm{B}}T_c = \frac{\langle\omega\rangle}{1.2} \exp\left[-\frac{1.04\,(1+\lambda)}{\lambda - \mu^*\,(1+0.62\lambda)}\right] \quad , \tag{2}$$

where λ is the attractive electron–phonon-induced interaction and μ^* is the renormalized Coulomb repulsion. In high-density atomic hydrogen, Ashcroft[15] demonstrated via an *ab initio* calculation that $\mu^* = 0.089$, which is remarkably close to $\mu^* = 0.085$ obtained from the Bennemann–Garland formula[17], both results similar to the somewhat standard value for a high-density system of $\mu^* \approx 0.1$. In this work, we therefore take $\mu^* = 0.089$ for estimating T_c. It should be noted that this approximation fails in molecular hydrogen[15], as investigated thoroughly in Refs. 20–22 using a specialized formulation of DFT for superconductivity where μ^* is calculated *ab initio*. Although, at high densities, μ^* is found to nonetheless be 0.08 (e.g., pressures just above 460 GPa, near molecular dissociation)[22].

For $\lambda \gtrsim 1.3$ (which in fact corresponds to the situations considered below), Eq. (2) often provides a lower bound to T_c. In this case, both a strong-coupling correction as well as a correction for the shape-dependence of T_c with $\langle\omega\rangle$ must be made. The first of these will be shown below to be especially important in atomic metallic hydrogen. These corrections are included in the Allen–Dynes equation[26],

$$k_{\mathrm{B}}T_c = f_1 f_2 \frac{\omega_{\mathrm{ln}}}{1.2} \exp\left[-\frac{1.04\,(1+\lambda)}{\lambda - \mu^*\,(1+0.62\lambda)}\right] \tag{3}$$

where ω_{ln} is the logarithmic average frequency [i.e., $\ln(\omega_{\mathrm{ln}}) = \langle\ln\omega\rangle$] and

$$f_1 = \left[1 + (\lambda/\Lambda_1)^{3/2}\right]^{1/3} \tag{4}$$

$$f_2 = 1 + \frac{(\bar{\omega}_2/\omega_{\mathrm{ln}} - 1)\,\lambda^2}{\lambda^2 + \Lambda_2^2} \tag{5}$$

denote the strong-coupling and shape corrections, respectively, where $\bar{\omega}_2 = \langle \omega^2 \rangle^{1/2}$ and Λ_1 and Λ_2 are fitting parameters (e.g., to full solutions of the Eliashberg equations).

In the original Allen–Dynes equation[26],

$$\Lambda_1 = 2.46 \left(1 + 3.8\mu^*\right) \tag{6}$$

$$\Lambda_2 = 1.82 \left(1 + 6.3\mu^*\right) \left(\bar{\omega}_2/\omega_{\mathrm{ln}}\right) \quad . \tag{7}$$

However, a least-squares analysis between T_c as predicted by Eq. (3) and that calculated numerically in the Eliashberg formalism for a fcc lattice of atomic metallic hydrogen at 2 TPa[17] suggests the following reparametrization

$$\Lambda_1 = 2.26 \left(1 - 1.28\mu^*\right) \tag{8}$$

$$\Lambda_2 = 2.76 \left(1 + 8.86\mu^*\right) \left(\bar{\omega}_2/\omega_{\mathrm{ln}}\right) \quad , \tag{9}$$

which interestingly provides more accurate values of T_c for a selection of low-temperature superconductors as well[17]. In passing, we note that there is a very recent further reparametrization[19] that appears especially well-suited for calculating T_c for a range of μ^* values (which could be useful for studying both the molecular and atomic phases concurrently, for example).

In this work, values of T_c are calculated using both Eqs. (2) and (3) as well as both parametrization for Λ_1 and Λ_2, in order to give a range of estimates for T_c.

III. COMPUTATIONAL DETAILS

All calculations were performed using the *ab initio* Quantum ESPRESSO (QE) DFT code[27]. A norm-conserving Troullier–Martins pseudopotential[28] with a core radius of 0.65 a.u. was used to replace the $1/r$ Coulomb potential of hydrogen. This radius was chosen to ensure no core-overlap up to the highest pressure considered in this work (3.5 TPa). The Perdew-Burke-Ernzerhof exchange and correlation functional[29] was used for all calculations. A basis set of plane waves with a cutoff of 120 Ry was also used, giving a convergence in energy to better than $\sim$0.2 mRy/proton, as well as 24^3 **k**-points for Brillouin-zone (BZ) sampling with the smearing scheme of Methfessel–Paxton[30] and a fictitious smearing temperature T of $k_{\mathrm{B}}T = 0.02$ Ry. Phonons were calculated using density functional perturbation theory as implemented within QE. Additional computational details pertaining to the calculations of phonons and electron–phonon interactions will be provided and discussed in Section V.

IV. GROUND-STATE STRUCTURES OF ATOMIC METALLIC HYDROGEN

In this section, the structural changes that occur in atomic metallic hydrogen as a function of pressure are discussed. On the basis of our previous study[3], we consider $I4_1/amd$ at pressures from 500 GPa to 1.5 TPa and $R\text{-}3m$ from 1 to 3.5 TPa. We first consider the lattice changes that occur (e.g., compression). We then consider the $I4_1/amd \rightarrow R\text{-}3m$ transition and discuss the vibrational properties of each structure that contribute to it, in anticipation of the results that are to follow in Section V. A further discussion of the ground-state and metastable structures of atomic metallic hydrogen can be found in Ref. 3.

A. Lattice Parameters

In terms of their primitive unit-cells, $I4_1/amd$ is tetragonal (with $a = b \neq c$) with two symmetry inequivalent atoms at Wyckoff positions $(0, 0, 1/2)$ and $(0, 1/2, 3/4)$, and $R\text{-}3m$ is hexagonal (also with $a = b \neq c$) and a single symmetry inequivalent atom at the origin. The lattice parameters of both structures can therefore be specified completely by a and the c/a ratio, as indicated in Fig. 1. For the pressure ranges under consideration, the lattice parameters and corresponding Wigner–Seitz radii r_s are shown in Tables I and II, respectively.

Between 500 – 700 GPa, $I4_1/amd$ resists compression along the c axis, as can be seen in the c/a ratio which increases from 2.545 to 2.764. Above 700 GPa, the resistance continues, but the compression becomes much more uniform. For example, by 1.5 TPa, the c/a ratio increases to only 2.849. In $R\text{-}3m$, on the other hand, the c/a ratio remains relatively constant in the middle of its stability range near $3.05 – 3.06$. However, near the predicted transition pressures of $\sim$1 and 3.5 TPa (see below and Ref. 3) there is a preferred compression along the c axis, in the latter case eventually compressing directly to fcc[3].

TABLE I: Lattice parameters and corresponding Wigner–Seitz radii r_s of $I4_1/amd$ as a function of pressure.

Pressure (TPa)	a (a.u.)	c/a	r_s (a.u.)
0.5	2.299	2.545	1.226
0.6	2.227	2.599	1.197
0.7	2.134	2.764	1.170
0.8	2.094	2.769	1.149
0.9	2.058	2.774	1.130
1.0	2.027	2.778	1.113
1.5	1.893	2.849	1.049

TABLE II: Lattice parameters and corresponding Wigner–Seitz radii r_s of R-3m as a function of pressure.

Pressure (TPa)	a (a.u.)	c/a	r_s (a.u.)
1.0	1.832	3.236	1.111
1.5	1.758	3.061	1.047
2.0	1.685	3.054	1.002
2.5	1.629	3.051	0.969
3.0	1.584	3.047	0.942
3.5	1.564	2.943	0.919

B. $I4_1/amd \to R$-3m Transition

Static-lattice enthalpy calculations indicate that $I4_1/amd$ transforms to R-3m near 2.5 TPa, but dynamic-lattice calculations (in the harmonic approximation) suggest that this pressure is significantly reduced to $\sim$1 TPa[3]. In this section, we use the harmonic and quasiharmonic approximations to further investigate the $I4_1/amd \to R$-3m transition, in anticipation of the results that are to follow in Section V.

Ground-state enthalpies for $I4_1/amd$ and R-3m (defined by the parameters in Tables I and II, respectively) were calculated at 1 and 1.5 TPa; Table III. ZPEs at each pressure were estimated using the harmonic approximation: $E_{\mathrm{ZPE}} = \int d\omega\ F(\omega)\hbar\omega/2$, where $F(\omega)$ is the phonon density of states (PHDOS), and are shown in Table III as well. Neglecting zero-point pressures (ZPPs) and making the simple approximation that the total enthalpies are given by $H + E_{\mathrm{ZPE}}$ (as was done in Ref. 3) suggests that the $I4_1/amd \to R$-3m transition occurs nearly midway between 1 and 1.5 TPa, which is very close to, but slightly higher than our original estimate of 1 TPa[3]. Going beyond this

TABLE III: Ground-state enthalpies and ZPEs of $I4_1/amd$ and R-3m at 1 and 1.5 TPa. Pressures P are in TPa and enthalpies and energies are in Ry/proton.

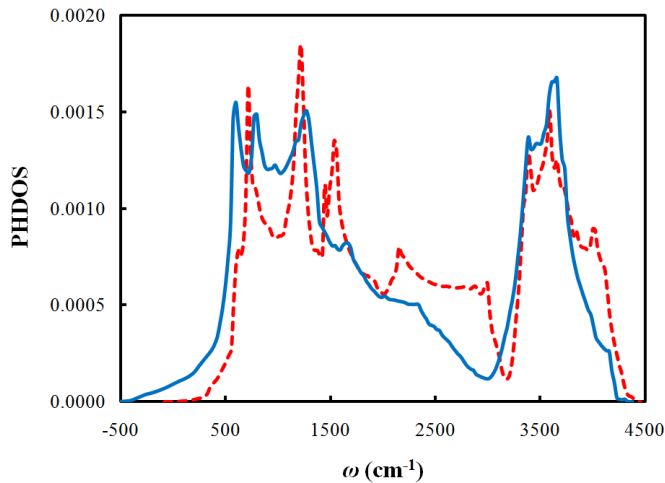|	$P = 1.0$	1.5
H		
$I4_1/amd$	-0.49955	-0.32022
R-3m	-0.49534	-0.31768
E_{ZPE}		
$I4_1/amd$	0.02708	0.03120
R-3m	0.02395	0.02769
$H + E_{\mathrm{ZPE}}$		
$I4_1/amd$	-0.47247	-0.28902
R-3m	-0.47140	-0.28999

FIG. 2: (color online). PHDOS of $I4_1/amd$ (dashed red line) and R-$3m$ (solid blue line) at 1.5 TPa. The results have been normalized by the number of atoms per primitive unit-cell. Negative values indicate imaginary frequencies (and thus instabilities, as discussed in the text).

approximation, the total enthalpies, including the ZPPs, can be estimated using a linear approximation,

$$H_{\text{tot}} = H_{\text{avg}} + E_{\text{ZPE, avg}} + p_{\text{ZPE}}V_{\text{avg}} \tag{10}$$

where

$$p_{\text{ZPE}} = -\frac{\partial E_{\text{ZPE}}}{\partial V} \tag{11}$$

is the ZPP, V is the volume, and the subscripts avg denote the average values of each quantity between 1 and 1.5 TPa. [Note that the latter two quantities in Eq. (10) correspond to the zero-point enthalpy.] Estimating p_{ZPE} using a simple finite difference gives total enthalpies of -0.35765 and -0.35976 Ry/proton for $I4_1/amd$ and R-$3m$, respectively, at 1.25 TPa. This suggests that the actual transition pressure is a bit lower than the simple enthalpy estimate, and is coincidentally in agreement with our original prediction of $\sim$1 TPa[3].

As can be inferred from Table III and the discussion above, the large decrease in the $I4_1/amd \rightarrow R$-$3m$ transition pressure from the static-lattice prediction ($\sim$2.5 TPa[3]) arises primarily from the significantly lower E_{ZPE} in R-$3m$ (as well as a smaller contribution from the lower p_{ZPE}). To help understand this, the PHDOS for both structures is shown in Fig. 2. It can be seen that there are three differences that lead to this behavior: (i) the density of high-frequency phonons is greater in $I4_1/amd$, and also occurs at higher frequencies (3180 – 4430 cm^{-1} vs 3000 – 4230 cm^{-1}); (ii) $I4_1/amd$ has a significant density of mid-frequency phonons ($\sim$1400 – 3000 cm^{-1}), while such modes are mostly absent in R-$3m$ (e.g., $I4_1/amd$ shows peaks at 1510, 2150, and 2990 cm^{-1}); and (therefore) (iii) the PHDOS of R-$3m$ is mostly concentrated at low frequencies ($\lesssim$ 1400 cm^{-1}).

In passing, we note that R-$3m$ shows a small density of imaginary phonon states at 1.5 TPa. Estimating the resulting energy within the harmonic approximation[3] shows that it integrates to $1.372 \cdot 10^{-5}$ Ry/proton. While this is within the accuracy of our calculations, this behavior is expected considering that it is indicative of instability in a lattice of ions treated classically; and classically, the $I4_1/amd \rightarrow R$-$3m$ transition occurs near 2.5 TPa[3], as discussed above. This is further confirmed by the fact that the instability goes to zero with increasing pressure, while such behavior begins to develop in $I4_1/amd$ – see Ref. 3. We will return to this point below.

Considering that the PHDOS are quite different between $I4_1/amd$ and R-$3m$ and it is finite-temperature effects that are focused on below (i.e., T_c), the possibility of vibrational entropic stabilization of one phase over the other exists. In order to estimate this, the quasiharmonic approximation can be used,

$$F(V,T) = E_0(V) + k_{\text{B}}T \int_0^\infty d\omega \; F(\omega) \ln\left[\sinh\left(\frac{\hbar\omega}{2k_{\text{B}}T}\right)\right] \tag{12}$$

where $F(V,T)$ is the Helmholtz free-energy and $E_0(V)$ is the static-lattice energy. From this, the Gibbs free energy G can be calculated via $G = F + pV$, given p. At $T = 0$K, p is given by the external pressure plus the ZPP [Eq. (11)]. However, for a fixed V, p is a function of T, due to thermal expansion of the lattice caused by anharmonic phonons. Contrary to the expectation that such effects may be large[31], calculations of the melting line of atomic
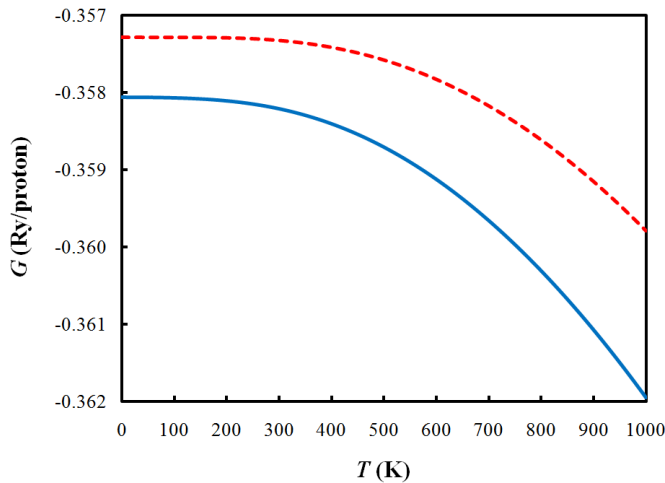
FIG. 3: (color online). G vs T for $I4_1/amd$ (dashed red line) and R-$3m$ (solid blue line) at 1.5 TPa.

metallic hydrogen (not shown)[32] indicate that thermal expansion is small, at least up to a few hundred K where the system is likely to melt anyway; and since the purpose of this discussion is just to understand qualitative changes that may arise at finite temperature, we can estimate p using the $T = 0$K value. Figure 3 shows the resulting estimates of G. Despite their remarkably different PHDOS, the behaviors of G with T are rather similar for both $I4_1/amd$ and R-$3m$. Thus, temperature is not expected to significantly affect the $I4_1/amd \rightarrow R$-$3m$ transition.

Based on these results, below we consider $I4_1/amd$ from 500 GPa to 1.5 TPa and R-$3m$ from 1 to 3.5 TPa, and, for the sake of discussion, the $I4_1/amd \rightarrow R$-$3m$ transition to occur between 1 and 1.5 TPa.

V. SUPERCONDUCTIVITY

In this section, we investigate superconductivity in the $I4_1/amd$ and R-$3m$ structures of atomic metallic hydrogen. We first provide relevant computational details not discussed in Section III, and convergence of the parameters necessary to evaluate Eqs. (2) and (3). We then present and discuss the calculated parameters and use them to calculate values of T_c.

A. Computational Details

In order to estimate T_c using Eqs. (2) and (3), $\langle \omega \rangle$, ω_{ln}, $\bar{\omega}_2$, and λ must all be determined. Of course, the frequency parameters can be calculated directly from the PHDOS. For example, $\langle \omega \rangle = (1/n_{\mathrm{ph}}) \int d\omega \, F(\omega)\omega$, where n_{ph} is the number of phonon modes and $\int d\omega \, F(\omega) = n_{\mathrm{ph}}$. In order to calculate λ, however, a (slowly convergent) double-delta integration must be performed on the Fermi surface – see Ref. 33 for a complete discussion and the precise implementation details within QE. In order to accurately perform this integration, very dense $\mathbf{k}$-point (electronic) and $\mathbf{q}$-point (phonon wave-vector) grids can be used with the delta functions approximated as Gaussians. For both the $I4_1/amd$ and R-$3m$ structures, we found that an electronic grid of 48^3 $\mathbf{k}$-points (and using 24^3 $\mathbf{k}$-points to calculate phonons, as discussed in Section III) gave convergence with no discernible error. Details of the $\mathbf{q}$-point grids will be given below. For both structures and each pressure considered, λ was calculated using Gaussian broadenings from 0.005 to 0.05 Ry in steps of 0.005 Ry. The values reported below were then chosen using the broadening for which λ appeared to be converged to within $\sim$0.05. In most cases, broadenings of $0.02 - 0.025$ Ry were sufficient. However, in a few cases (e.g., R-$3m$ at and above 2 TPa), broadenings of up to $\sim$0.035 Ry were used.

In order to determine a sufficient density for the $\mathbf{q}$-point grids (used also for the phonon calculations), a series of calculations with 1^3, 2^3, 4^3, 6^3, and 8^3 $\mathbf{q}$-points were performed, using $I4_1/amd$ at 500 GPa as a test case (we also considered R-$3m$ at 2 TPa – not shown). It should be kept in mind that such rigorous testing with respect to $\mathbf{q}$-points is especially important in atomic metallic hydrogen with large values of λ, as inadequate sampling has been shown to cause significantly incorrect results[13,14]. In fact, our calculations below suggest that the results of a recent study[18] considering Cs-IV (which also has the $I4_1/amd$ structure), over a more narrow pressure range than considered here using only 3^3 $\mathbf{q}$-points gives somewhat incorrect values for λ, both in magnitude and its trend with pressure. The

TABLE IV: Convergence of $\langle\omega\rangle$, ω_{ln}, and λ with the number of **q**-points for $I4_1/amd$ at 500 GPa.

No. of **q**-points	$\langle\omega\rangle$ (K)	ω_{ln} (K)	λ
1^3	1660	1438	17.91
2^3	2307	1953	2.82
4^3	2277	2031	2.06
6^3	2287	1997	1.67
8^3	2295	2068	1.81
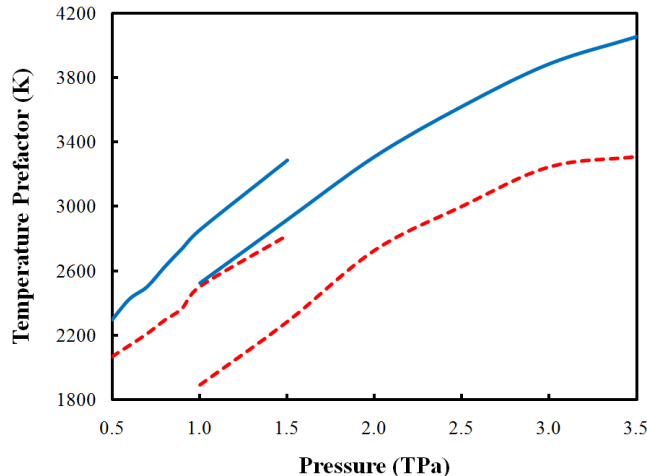
FIG. 4: (color online). Temperature prefactors $k_B\langle\omega\rangle$ (solid blue line) and $k_B\omega_{\text{ln}}$ (dashed red line) as a function of pressure in atomic metallic hydrogen.

values of λ for the various densities of **q**-points, as well as values of $\langle\omega\rangle$ and ω_{ln}, are shown in Table IV. (Note that for all calculations, the dense electronic grid containing 48^3 **k**-points was used.) Relative convergence in λ is seen to require at least 6^3 **q**-points (to be within 10% of the converged value, for example). This is likely due to Fermi surface "hot spots" that have been shown to exist in other alkali metals[34], which can significantly contribute to the electron–phonon interaction. Table IV also shows, on the other hand, that $\langle\omega\rangle$ and ω_{ln} achieve relative convergence with as little as 2^3 **q**-points, which is consistent with the density found necessary in our previous work to accurately calculate the PHDOS (for ZPEs) of the structures of atomic metallic hydrogen[3].

Below, 8^3 **q**-points were used for all calculations (as well as those previously discussed in Section IV), corresponding to 59 and 150 total **q**-points in the irreducible BZs for $I4_1/amd$ and R-$3m$, respectively.

B. Superconducting Parameters

As shown in Fig. 4, $\langle\omega\rangle$ and ω_{ln} are both extremely high, and increase significantly with pressure[3]; $\langle\omega\rangle$ increases from 2295K to 4056K as the pressure is increased from 500 GPa to 3.5 TPa, and while ω_{ln} is significantly less (especially for R-$3m$), it nonetheless increases from 2068K to 3308K over the same range. Furthermore, there is a significant decrease in both $\langle\omega\rangle$ and ω_{ln} at the $I4_1/amd \rightarrow R$-$3m$ transition (e.g., by 765K and 926K, respectively, at 1.5 TPa), consistent with the results and discussion in Section IV B.

More interesting is the behavior of λ with pressure; Fig. 5. Near molecular dissociation ($\sim$500 GPa), the values of λ in both the atomic and molecular phases are remarkably close. In $I4_1/amd$, $\lambda \approx 1.81$ (see also Table IV), and in the molecular phase ($Cmca$), $\lambda \approx 2$ just above 460 GPa, but appears to slowly decrease with increasing pressure – see Refs. 20 and 22. Thus, given that λ and μ^* are similar in both phases near molecular dissociation (see again Section II for a discussion of μ^*), a nearly continuous variation in T_c is likely to occur with increasing pressure in this range.

A large increase in λ is seen to occur between 500 – 700 GPa, from 1.81 to 2.32. To help understand this, the electron–phonon spectral function, $\alpha^2F(\omega)$, at 500 GPa is compared to that at 700 GPa in Fig. 6. It can be seen that there is an increase in coupling to both the low and high-frequency phonon modes as the atomic phase stabilizes, while there is relatively little change in the coupling to those at mid frequency. The former increase is unexpected,
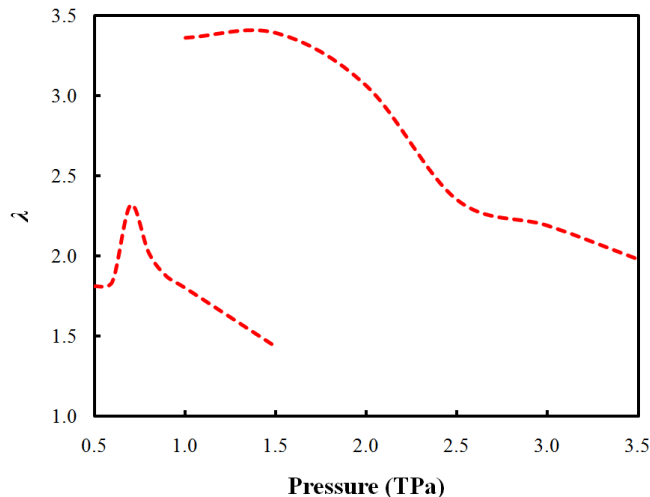
FIG. 5: (color online). Electron–phonon-induced interaction λ as a function of pressure in atomic metallic hydrogen.
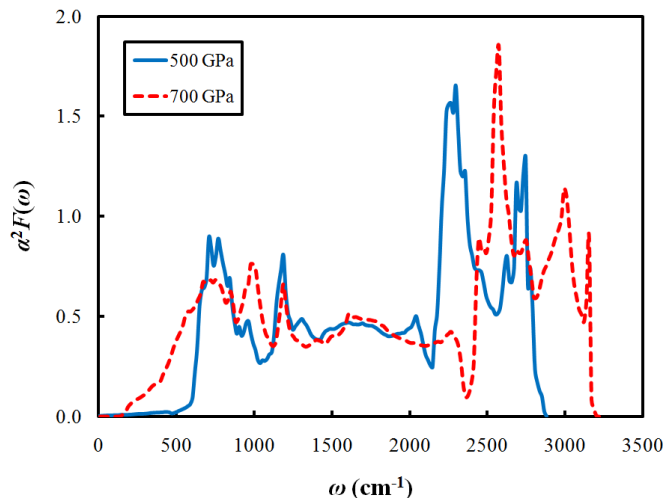

FIG. 6: (color online). Electron–phonon spectral function $\alpha^2 F(\omega)$ for $I4_1/amd$ at 500 and 700 GPa.

as with increasing pressure the PHDOS shifts to higher frequencies, as is indicated in Fig. 4. The sharp increase in λ, along with the increased $\langle \omega \rangle$ and $\omega_{\ln}$ (see again Fig. 4), suggests that a correspondingly large increase in T_c should occur over this small pressure range, which is shown below to indeed be the case.

Figure 6 also shows that significant electron–phonon coupling occurs into modes at all frequencies. This suggests that the large value of λ is primarily due to the electron–ion interaction being the bare (unscreened) Coulomb attraction, which was one of the reasons for the original prediction of high-T_c superconductivity in hydrogen[5]. Although, there does appear to be slight additional coupling into the high-frequency modes. In order to understand this, phonon dispersion curves and linewidths γ (the latter directly proportional to $\lambda \omega$) for $I4_1/amd$ at 700 GPa are shown in Figs. 7 and 8, respectively. The linewidths are seen to be largest for the high-frequency modes at the Γ point (or close to it). This suggests that the strongest electron–phonon coupling arises from local vibrations (e.g., those within each unit cell). Such vibrations are likely to result in the largest variation of the potential, consistent with the suggestion above that the large value of λ is primarily due to the bare Coulomb attraction.

At the $I4_1/amd \rightarrow R\text{-}3m$ transition near 1.5 TPa, a large jump in λ occurs, from 1.43 to 3.39. This can be understood by comparing $\alpha^2 F(\omega)$ for both structures; Fig. 9. In $R\text{-}3m$, the large value of λ is seen to occur from a strong coupling into the low-frequency modes $[\lambda = 2 \int d\omega \; \alpha^2 F(\omega)/\omega]$. This appears to be primarily due to the correspondingly high PHDOS at low frequencies (see also below), which is absent in $I4_1/amd$ (see again Section IV B). (Comparing Figs. 6 and 9 also shows that in $I4_1/amd$ there is a decrease in coupling into all modes with an increase in pressure above 700 GPa, especially at low frequencies.)

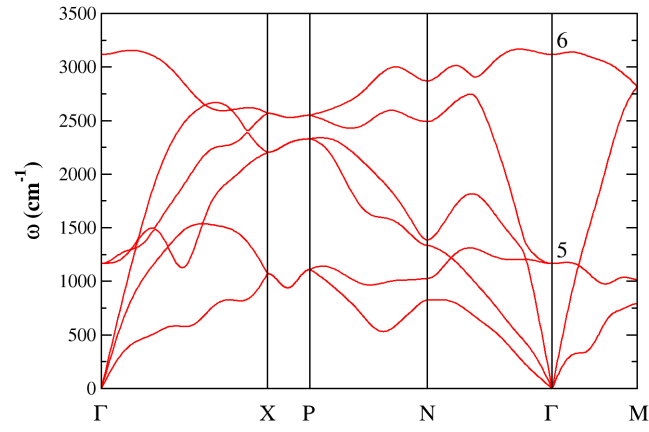Insight into the large electron–phonon coupling with the low-frequency modes in $R\text{-}3m$ can be obtained again from

FIG. 7: (color online). Phonon dispersion curves for $I4_1/amd$ at 700 GPa. The numbers 5 and 6 denote the highest-frequency phonon modes at Γ.
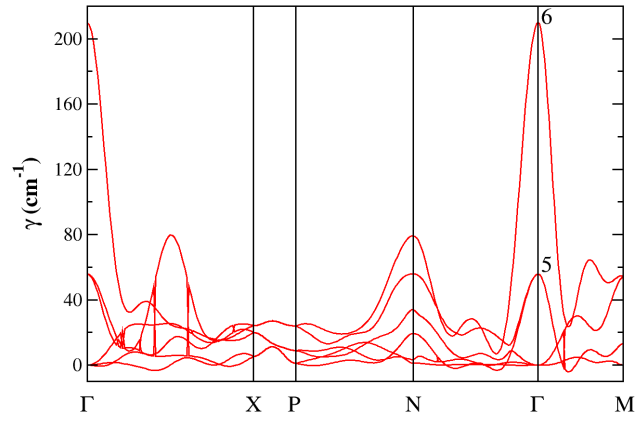

FIG. 8: (color online). Phonon linewidths for $I4_1/amd$ at 700 GPa. The numbers 5 and 6 denote the linewidths corresponding to coupling to the highest-frequency phonon modes at Γ.
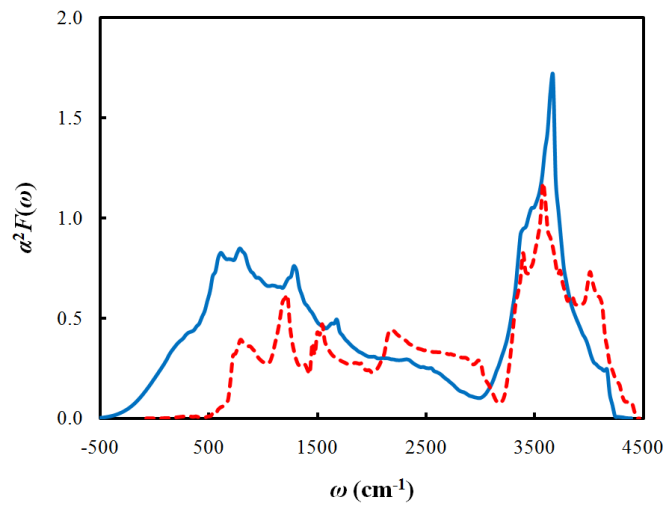

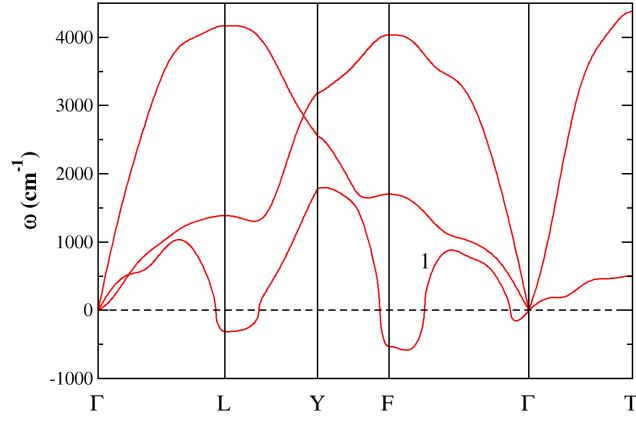FIG. 9: (color online). Electron–phonon spectral function $\alpha^2F(\omega)$ for $I4_1/amd$ (dashed red line) and $R\text{-}3m$ (solid blue line) at 1.5 TPa.

FIG. 10: (color online). Phonon dispersion curves for R-$3m$ at 1.5 TPa. Negative values correspond to imaginary frequencies and indicate instabilities, as discussed in the text. The lowest-frequency (and unstable) mode is denoted using the number 1.
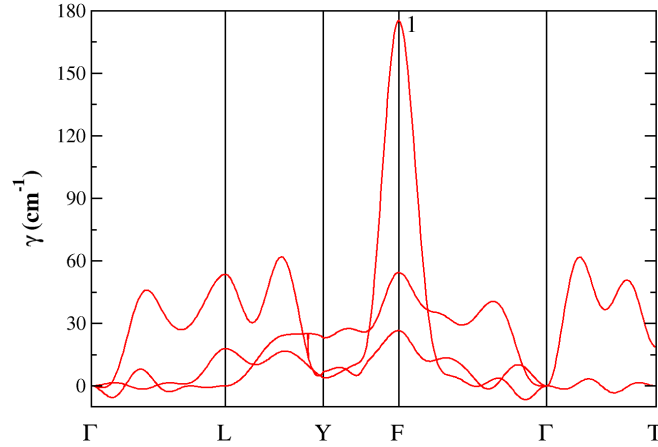

FIG. 11: (color online). Phonon linewidths for R-$3m$ at 1.5 TPa. The linewidth corresponding to coupling to the unstable phonon mode is denoted using the number 1.

phonon dispersion curves and γ, as shown in Figs. 10 and 11 at 1.5 TPa. Large imaginary frequencies at the L and F points of the BZ show that R-$3m$ has significant lattice instabilities, which is expected when the protons are treated classically – see Section IV B and Ref. 3. Furthermore, Fig. 11 shows that the strongest electron–phonon coupling occurs near the F point. These results suggest that, at the F point, the lattice instability and strong electron–phonon coupling are directly related, indicative of polaron formation. This analysis is consistent with that in Ref. 16, where λ values as high as ~ 7.32 calculated for the fcc lattice near 2 TPa[16,17] were attributed to the lattice being close to unstable and strong coupling with the low-frequency (possibly unstable) modes. (Note also that fcc has an even higher PHDOS at low frequencies compared to R-$3m$[3].)

With increasing pressure, λ in R-$3m$ decreases from its maximum to ~ 1.98 by 3.5 TPa. Figure 12 shows that this results from a weakened coupling into the low-frequency modes that was responsible for the sharp increase in λ in the first place (near the $I4_1/amd \rightarrow R$-$3m$ transition). This is likely due to an overall decrease in the PHDOS at low frequencies with increasing pressure (not shown), as the lattice (of classical ions) stabilizes[3].

C. T_c Values

Using the parameters in Figs. 4 and 5, Eqs. (2) and (3) were used to calculate T_c; Fig. 13. They are seen to be remarkably high, but nonetheless consistent with the discussion above. The Allen–Dynes equation and its reparametrization[17], in most cases, give much higher estimates than the McMillan formula (as expected, based on the discussion in Section II). Given that $\omega_{\ln}$ is significantly less than $\langle \omega \rangle$, the increase is thus due entirely to the correction factors f_1 and f_2. Comparing these, in a number of cases, shows that it is f_1 (the strong-coupling correction) that is most important, especially in the reparametrized Allen–Dynes equation[17]. For example, at 700 GPa $f_1 \approx 1.31$ and
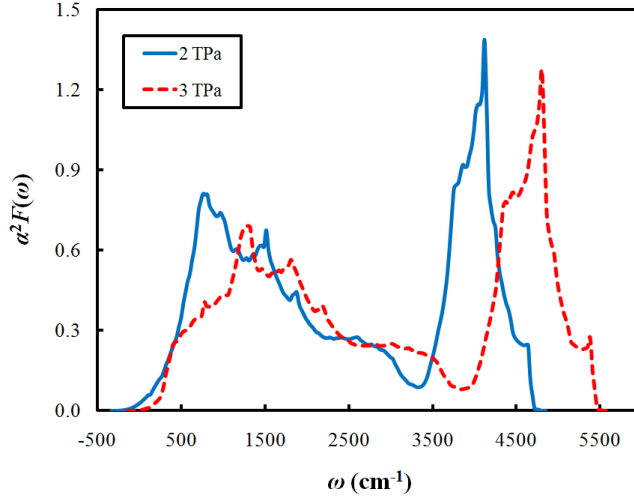
FIG. 12: (color online). Electron–phonon spectral function $\alpha^2 F(\omega)$ for R-$3m$ at 2 and 3 TPa.
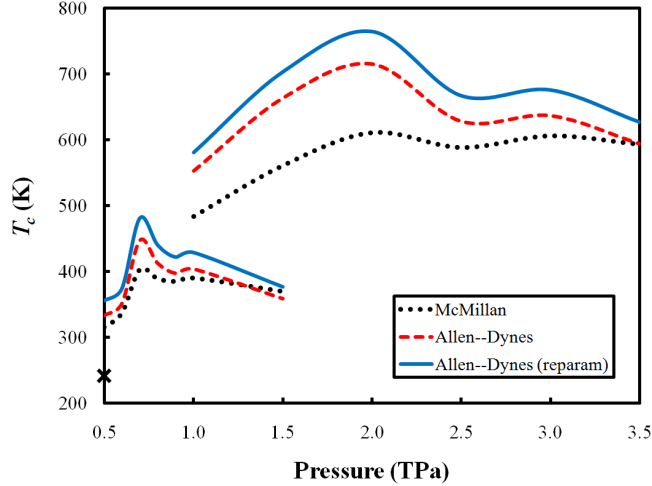

FIG. 13: (color online). Values of T_c for atomic metallic hydrogen calculated using Eqs. (2) and (3). The estimated value of T_c for the high-pressure molecular phase[20–22] is shown as **x**.

$f_2 \approx 1.03$.

Just above molecular dissociation, $T_c \approx 315 - 356$K. The increase in λ combined with increases in $\langle\omega\rangle$ and $\omega_{\ln}$ with pressure cause T_c to increase up to $403 - 481$K by 700 GPa. With increasing pressure, T_c then decreases (in the $I4_1/amd$ phase). However, at the $I4_1/amd \to R$-$3m$ transition, a large jump in T_c occurs, from $370 - 377$K to $561 - 703$K. This is due entirely to the jump in λ, considering that $\langle\omega\rangle$ and $\omega_{\ln}$ are significantly lower in R-$3m$ compared to $I4_1/amd$ (see Fig. 4). Although, with increasing pressure, T_c again decreases. It is interesting to note that secondary maxima in T_c occur in both $I4_1/amd$ and R-$3m$. Given that there appears to be monotonic decreases in λ above their maxima in both structures (see Fig. 5), this behavior is simply due to an interplay between λ and $\langle\omega\rangle$ or $\omega_{\ln}$. In any event, $\sim$764K represents an approximate upper bound to T_c in atomic metallic hydrogen, and possibly conventional superconductors altogether (i.e., those described by BCS theory).

VI.   CONCLUSIONS

In conclusion, we investigated superconductivity in the ground-state structures of atomic metallic hydrogen over the range 500 GPa to 3.5 TPa. Near molecular dissociation, the electron–phonon coupling λ and renormalized Coulomb repulsion in the atomic phase were demonstrated to be similar to the values in the molecular phase. This suggests a nearly continuous increase in T_c with pressure during the molecular-to-atomic transition, to $\sim$356K near 500 GPa.

As the atomic phase stabilizes with increasing pressure, λ increases, causing T_c to increase to $\sim$481K near 700 GPa. Near the first atomic–atomic structural phase transformation near 1.5 TPa, a large jump in λ occurs due to a high PHDOS at low frequencies, causing T_c to increase to as high as 764K.

While the T_c values presented in this work seem incredibly high, they are nonetheless reasonable. However, there are two caveats. First of all, even the lowest pressures considered in this work are higher than those currently obtainable in low-temperature experiments ($\sim$342 GPa[35]). Nonetheless, all of them are important to planetary physics (albeit in most cases at temperatures higher than the calculated values of T_c). The other caveat is that it is quite possible that the T_c values are even higher than the melting temperatures. However, this suggests the interesting possibility that the atomic metallic solid phases of hydrogen (at least the $I4_1/amd$ and $R\text{-}3m$ structures) exist entirely in superconducting states.

Acknowledgments

* mcmahonj@illinois.edu

† ceperley@ncsa.uiuc.edu

[1] E. Wigner and H. B. Huntington, J. Chem. Phys. **3**, 1748 (1935).

[2] C. J. Pickard and R. J. Needs, Nature Phys. **3**, 473 (2007).

[3] J. M. McMahon and D. M. Ceperley, Phys. Rev. Lett. **106**, 165302 (2011).

[4] M. Städele and R. M. Martin, Phys. Rev. Lett. **84**, 6070 (2000).

[5] N. W. Ashcroft, Phys. Rev. Lett. **21**, 1748 (1968).

[6] J. Bardeen, L. N. Cooper, and J. R. Schrieffer, Phys. Rev. **108**, 1175 (1957).

[7] T. Schneider and E. Stoll, Physica **55**, 702 (1971).

[8] L. G. Caron, Phys. Rev. B **9**, 5025 (1974).

[9] R. P. Gupta and S. K. Sinha, in *Superconductivity in d- and f-band Metals*, edited by D. H. Douglass (Plenum: New York, 1976), pp. 583–592.

[10] A. C. Switendick, in *Superconductivity in d- and f-band Metals*, edited by D. H. Douglass (Plenum: New York, 1976), pp. 593–605.

[11] M. D. Whitmore, J. P. Carbotte, and R. C. Shukla, Can. J. Phys. **57**, 1185 (1979).

[12] B. I. Min, H. J. F. Jansen, and A. J. Freeman, Phys. Rev. B **30**, 5076 (1984).

[13] T. W. Barbee III, A. García, and M. L. Cohen, Nature **340**, 369 (1989).

[14] T. W. Barbee III and M. L. Cohen, Phys. Rev. B **43**, 5269 (1991).

[15] C. F. Richardson and N. W. Ashcroft, Phys. Rev. Lett. **78**, 118 (1997).

[16] E. G. Maksimov and D. Y. Savrasov, Solid State Commun. **119**, 569 (2001).

[17] R. Szczęśniak and M. W. Jarosik, Solid State Commun. **149**, 2053 (2009).

[18] Y. Yan, J. Gong, and Y. Liu, Phys. Lett. A **375**, 1264 (2011).

[19] R. Szczęśniak and M. W. Jarosik (2011), URL http://arxiv.org/abs/1105.5527.

[20] P. Cudazzo, G. Profeta, A. Sanna, A. Floris, A. Continenza, S. Massidda, and E. K. U. Gross, Phys. Rev. Lett. **100**, 257001 (2008).

[21] P. Cudazzo, G. Profeta, A. Sanna, A. Floris, A. Continenza, S. Massidda, and E. K. U. Gross, Phys. Rev. B **81**, 134505 (2010).

[22] P. Cudazzo, G. Profeta, A. Sanna, A. Floris, A. Continenza, S. Massidda, and E. K. U. Gross, Phys. Rev. B **81**, 134506 (2010).

[23] M. Hanfland, K. Syassen, N. E. Christensen, and D. L. Novikov, Nature **408**, 174 (2000).

[24] W. L. McMillan, Phys. Rev. **167**, 331 (1968).

[25] R. C. Dynes, Solid State Commun. **10**, 615 (1972).

[26] P. B. Allen and R. C. Dynes, Phys. Rev. B **12**, 905 (1975).

[27] P. Giannozzi, S. Baroni, N. Bonini, M. Calandra, R. Car, C. Cavazzoni, D. Ceresoli, G. L. Chiarotti, M. Cococcioni, I. Dabo, *et al.*, J. Phys. Condens. Matter **21**, 395502 (2009), URL http://www.quantum-espresso.org.

[28] N. Troullier and J. L. Martins, Phys. Rev. B **43**, 1993 (1991).

[29] J. P. Perdew, K. Burke, and M. Ernzerhof, Phys. Rev. Lett. **77**, 3865 (1996).

[30] M. Methfessel and A. T. Paxton, Phys. Rev. B **40**, 3616 (1989).

[31] V. Natoli, R. M. Martin, and D. M. Ceperley, Phys. Rev. Lett. **70**, 1952 (1993).

[32] J. M. McMahon, M. A. Morales, C. Pierleoni, and D. M. Ceperley, in preparation (2011).

[33] M. Wierzbowska, S. de Gironcoli, and P. Giannozzi (2006), URL http://arxiv.org/abs/cond-mat/0504077.

[34] D. Kasinathan, J. Kuneš, A. Lazicki, H. Rosner, C. S. Yoo, R. T. Scalettar, and W. E. Pickett, Phys. Rev. Lett. **96**, 047004 (2006).

[35] C. Narayana, H. Luo, J. Orloff, and A. L. Ruoff, Nature **393**, 46 (1998).